Lab on a Chip

Cite this: *Lab Chip*, 2012, **12**, 4287–4295

www.rsc.org/loc

PAPER

Systematic characterization of feature dimensions and closing pressures for microfluidic valves produced *via* photoresist reflow†

P. M. Fordyce,*[ab] C. A. Diaz-Botia,[c] J. L. DeRisi[ab] and R. Gomez-Sjoberg*[ac]

Received 27th April 2012, Accepted 9th July 2012
DOI: 10.1039/c2lc40414a

Multilayer soft lithography (MSL) provides a convenient and low-cost method for fabricating poly(dimethyl siloxane) (PDMS) microfluidic devices with on-chip valves for automated and precise control of fluid flow. MSL casting molds for flow channels typically incorporate small patches of rounded positive photoresist at valve locations to achieve the rounded cross-sectional profile required for these valves to function properly. Despite the importance of these rounded features for device performance, a comprehensive characterization of how the rounding process affects feature dimensions and closing pressures has been lacking. Here, we measure valve dimensions both before and after rounding and closing pressures for 120 different valve widths and lengths at post-rounding heights between 15 and 84 μm, for a total of 1200 different geometries spanning a wide range of useful sizes. We find that valve height and width after rounding depend strongly on valve aspect ratios, with these effects becoming more pronounced for taller and narrower features. Based on the measured data, we provide a simple fitted model and an online tool for estimating the pre-rounding dimensions needed to achieve desired post-rounding dimensions. We also find that valve closing pressures are well explained by modelling valve membranes in a manner analogous to a suspension bridge, shedding new light on device physics and providing a practical model for estimating closing pressures during device design.

Introduction

Microfluidic devices fabricated in poly(dimethyl siloxane) (PDMS) by multilayer soft lithography (MSL)[1,2] have been used for a wide variety of applications, such as single-cell genomics[3] and transcriptomics,[4] protein crystallography,[5] high-throughput screening,[1] transcription factor binding assays,[6,7] and cell culture.[8] In these devices, dead-end channels in one layer of the device (“control channels”) are routed to cross channels containing experimental reagents in another layer (“flow channels”), forming a thin membrane between them at their intersection (Fig. 1A). Increasing the pressure in a control channel deflects this thin membrane, thereby restricting fluid flow within the flow channel and creating a pressure-activated valve (Fig. 1B). Such valves provide precise control over fluid flow within devices, and can be combined to form a variety of complex structures, including pumps,[9] mixers,[10,11] and multiplexers/demultiplexers.[9,12]

Devices can be configured in two geometries: “push-down”, in which flow channels are located below control channels, and “push-up”, in which flow channels are located above control channels (Fig. 1B). “Push-down” configurations allow flow channels to be in direct contact with a substrate, facilitating applications in which the substrate surface is modified and/or patterned before mounting the microfluidic device.[6,7] Closing pressures depend on valve dimensions and the thickness of the membrane separating the channels for both configurations;[13,14] however, higher pressures are required to close “push-down” valves, limiting the maximum flow channel height of these devices.[2,13,14] The lower pressures required to close “push-up” valves allow construction of devices with much taller channels, providing lower fluidic resistances and facilitating manipulation of cells,[8] beads, droplets, and other large objects.

In both configurations, the performance of these valves is highly dependent on the cross-sectional profile of the flow channel. If the flow channel has a cross section with sharp corners at a valve location, the membrane is not able to completely seal the corners, creating a “sieve” that can be opened and closed on command (Fig. 1B). Although such sieve valves can be very useful for trapping beads (to create chromatography columns,[15] for example) or changing the fluidic resistance of a channel, they cannot control fluid flow within the device. To produce fully sealing valves, flow channels must have a rounded cross-sectional profile at the point where the valve is formed (Fig. 1B).[9] Rounded profiles are typically generated using a positive

[a]*Department of Biochemistry and Biophysics, University of California San Francisco, 1700 4th Street Byers Hall Room 403, San Francisco, CA, 94158, USA. E-mail: polly@derisilab.ucsf.edu*
[b]*Howard Hughes Medical Institute, 4000 Jones Bridge Road, Chevy Chase, MD, 20815-6789, USA*
[c]*Engineering Division, Lawrence Berkeley National Laboratory, 1 Cyclotron Road Mail Stop 70A3362, Berkeley, CA, 94720-8178, USA. E-mail: RGomez@lbl.gov*
† Electronic supplementary information (ESI) available. See DOI: 10.1039/c2lc40414a

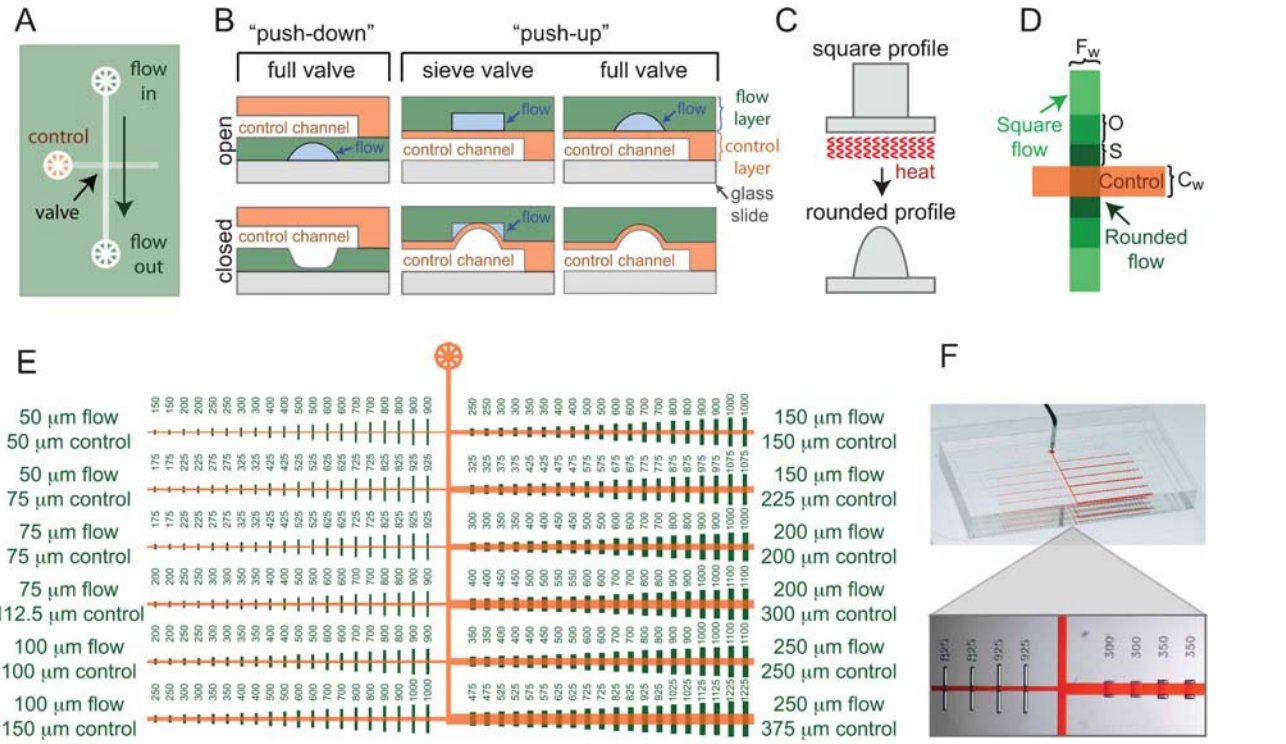

Fig. 1 Experimental geometries. (**A**) Top view of an MSL valve. (**B**) Side view of two-layer "push-down" and "push-up" devices. Pressurization of control channel deflects membrane separating the layers, closing valve (compare top and bottom). Valves with square flow channel profiles leave pockets of fluid flow (blue), creating a sieve ("push-up" configuration, left column). Valves with rounded flow channel profiles seal completely ("push-up" configuration, right column). (**C**) Slow heating of square channels made of positive photoresist allows reflow. (**D**) Rounded photoresist feature widths should match flow channel width (F_w); lengths are defined by control channel width (orange, C_w), spacing between rounded (dark green) and square (light green) photoresists (S), and overlap between photoresists (O). (**E**) Device design including 240 different valves of 6 different widths and varying lengths. (**F**) Photograph of device with detail showing individual channels.

photoresist (*e.g.* AZ50 XT or SPR 220) that is melted and reflowed by heating after photolithographic patterning, causing the initial rectangular cross-section to become parabolic (Fig. 1C).

Rounding complex continuous channel geometries made with thick ($> \sim 20$ μm) positive resist often leads to large variations in channel heights because of capillarity-driven movements of molten photoresist from one area of the design to another. Therefore, MSL flow molds with tall channels are typically composed of "rounding" positive photoresist patches only where valves are required, and SU-8 negative photoresists everywhere else (Fig. 1D). To avoid sharp changes in channel height that could result in dead volumes and edges that could trap particles or cells, the reflowed valve dimensions should match the dimensions of the surrounding SU-8 channel heights as closely as possible. Matching channel profiles can be particularly difficult for applications requiring relatively tall channels, where reflow can drastically change channel dimensions.

To establish a practical guide for the design of these devices, we systematically characterized the reflow process for a variety of microfluidic valve dimensions. Importantly, the range of feature geometries tested here encompasses all feature dimensions likely to be used within microfluidic devices requiring tall channels (20 to 85 μm). We demonstrate that for tall valves, final feature heights and widths after reflow are strongly dependent on design geometry. In addition, we determine that the closing valve pressures for these same valve geometries can be well described by a single physical "thick spring" model.[14] The data and software design tool presented here should prove a valuable resource for microfluidics laboratories seeking to optimize photoresist processing protocols and device design.

Methods

PDMS molding master fabrication

PDMS molding masters were made using 4″ test-grade silicon wafers (University Wafer, South Boston, MA). To improve adhesion of the photoresist patterns, both flow and control molds were first coated with a 5 μm layer of SU-8 2005 photoresist (Microchem Corp., Newton, MA) according to the manufacturer's instructions. Control mold features were then fabricated from SU-8 2025 (Microchem Corp.) according to the manufacturer's instructions. For flow mold production, wafers were coated with AZ Electronic Materials AZ50 XT photoresist (Capitol Scientific, Austin, TX) using a 3 step spin process (G3P-8 spinner, Specialty Coating Systems, Indianapolis, IN): (1) 500 rpm for 5 s with a 5 s ramp (spread), (2) 500 rpm, 750 rpm, 1000 rpm, 1250 rpm, or 1500 rpm for 30 s with a 5 s ramp (casting), (3) casting spin speed plus 2000 rpm for 1 s with a 1 s ramp (edge bead removal). Following photoresist deposition, wafers sat at room temperature for 20 min on a flat horizontal surface to ensure layer uniformity. Wafers were then placed directly on an aluminum-top hot plate (HS40A, Torrey Pines

Scientific, Carlsbad CA) set to ramp from 65 °C to 112 °C at 240 °C h^{-1}, followed by a variable time at 112 °C: 40 min for the 500 rpm wafers, 25 min for the 750 rpm and 1000 rpm wafers, and 20 min for the 1250 rpm and 1500 rpm wafers. The hot plate was allowed to cool on its own to ~40 °C or less before removing the wafers (to reduce photoresist cracking), and the wafers were then rehydrated overnight at room temperature. After rehydration, the wafers were exposed using a standard i-line photolithography mask aligner (Quintel Q2001CT, Neutronix-Quintel, Morgan Hill, CA). The exposures used were 3 × 30 s, 3 × 25 s, 3 × 22 s, 3 × 20 s, and 3 × 18 s for the 500, 750, 1000, 1250, and 1500 rpm wafers, respectively. Immediately after exposure, the wafers were developed in a 1 : 3 solution of AZ Electronic Materials AZ 400 K developer (Capitol Scientific), and then reflowed on an aluminum-top hot plate set to ramp from 65 °C to 190 °C at 10 °C h^{-1}, remaining at 190 °C for 4 h. This slow ramp is important to reduce the distortion of the patterns during reflow.

PDMS device fabrication

To ensure easy PDMS release, all molds were first silanized by exposing them to trichloromethylsilane (Sigma-Aldrich, St. Louis, MO) vapors for 60 min. Each flow mold was then coated with a 4 mm thick layer of Momentive Materials RTV 615 (R. S. Hughes, Oakland, CA) at a ratio of 1 : 5 (cross-linker : elastomer base) mixed using a Thinky AR-250 planetary centrifugal mixer (Thinky USA Inc., Laguna Hills, CA) (mixed for 5 min at 2000 rpm, debubbled for 3 min at 2200 rpm). The PDMS on the flow molds was then degassed in a vacuum chamber for at least 60 min. Both control molds and 2″ × 3″ glass slides were spin coated with a 1 : 20 mixture of RTV 615 components that had been mixed for 3 min at 2000 rpm and debubbled for 6 min at 2200 rpm. This RTV 615 mixture was initially spread onto the control molds and glass slides at 500 rpm for 5 s with a 5 s ramp and then spun at 1900 rpm for 60 s with a 15 s ramp. Flow molds were baked at 80 °C for 1 h, control molds were baked for 40 min, and glass slides were baked for only 20 min. Following baking, PDMS flow layers were peeled from the molds, cut to size, and aligned to control layers remaining on their molds. These aligned devices were baked for 1 h, cut from the control molds, punched to create control access ports using a punching press (Technical Innovations, Brazoria, TX), and placed on the coated glass slides. This final assembly was then baked at 80 °C for 1–12 h.

Characterization of valve dimensions *via* profilometry

All profiles were measured using a XP-2 profilometer (KLA-Tencor, Milpitas, CA) with a 0.02 mg stylus force. Profilometer measurements of pre-bake valve profiles were complicated by the fragility of the photoresist; consequently, we only measured heights for 4 valves per valve width per spin speed before baking (as opposed to 40 valve measurements after baking). Device widths and heights were determined automatically from the measured profiles using custom software written in Python.

Characterization of valve dimensions *via* image analysis

Valve images were captured using a Nikon stereoscope and analyzed using a custom algorithm written using the Image Processing Toolbox in Matlab (The Mathworks Inc., Natick, MA). In these images, valves appeared lighter than the surrounding wafer, permitting automated identification and dimension analysis *via* a two-step process. In the first step, valve regions were identified by thresholding pixel intensities using a high threshold and selecting only those regions large enough to be valves with the expected shape. In the second step, the threshold was lowered to identify the full extent of the valve and determine dimensions. After hard baking, the contrast between the valves and the surrounding wafer decreased and the feature boundaries became less regular; therefore, all post-bake valve dimensions were manually checked to ensure accuracy.

Characterization of membrane thickness *via* image analysis

Average valve membrane thickness was determined by slicing devices with a razor across valves to create a thin cross-sectional slice, imaging the slice with an inverted microscope, and analyzing the images using ImageJ software. Ten valves were imaged from 4 different devices, yielding an average thickness of 15.3 ± 2.5 μm (mean ± standard deviation).

Measurement of closing pressures

Valve closing pressures were measured by filling the microfluidic control channels with water and pressurizing them with regulated compressed air. A computer-controlled multi-channel pressure controller (MFCS, Fluigent, Paris, France) was used for pressures below 89.6 kPa (13 psi), while a manual regulator with an analog gauge (IR-2010, SMC Corp. of America, Noblesville, IN) was used for pressures between 89.6 kPa and 413.7 kPa (60 psi). Pressures to all valves on a device were incremented in steps of 1.72 kPa (0.25 psi) up to 89.6 kPa (13 psi), then in steps of 6.9 kPa (1 psi) until all valves were closed or the limit of the manual regulator was reached (89.6 kPa); valves were visually monitored *via* microscopy to determine their closing pressures. Closed valves were easily identified from the microscope image (Fig. 5).

Membrane deflection models

We compared measured closing pressures with pressures predicted by three previously derived models:[14] a "thick beam" model, a "thin spring" model, and a "thick spring" model. The thin spring and thick spring models presented here are similar to those derived previously, but extend the formalism to describe taller channels.

Thick beam model. In the thick beam model, each valve dimension is modelled as a pair of rigid beams joined in the middle.[14] As previously derived, this model predicts the following dependence of closing pressure (P) on valve dimensions (H = flow channel height; h = membrane width; W = valve width across channel; L = valve length along channel)

$$P = E[4Hh^3(W^{-4} + L^{-4})] \quad (1)$$

Here and in the other pressure models, E represents the experimentally measured Young's modulus for the PDMS that forms the valve membrane.

Thin spring model. In the thin spring model, the valve membrane is treated as a one-dimensional spring composed of

a semi-liquid slab, such that the pressure outside the slab is equal to the stress multiplied by the strain within the material:

$$P = E\varepsilon \quad (2)^{14}$$

The strain can be expressed as the difference between the path length of the membrane when pressurized and the path length of the membrane at rest:

$$\varepsilon = (l - W)/l \quad (3)$$

The profilometry measurements suggest that the path traveled by the membrane is approximately parabolic:

$$y = H - \frac{4H}{W^2}x^2 \quad (4)$$

Integrating along this path to determine a pressurized path length yields:

$$l = \frac{W^2}{8H}\left[\frac{4H}{W}\sqrt{\frac{32H^2}{W^2}+1} + \operatorname{arcsin h}\left(\frac{4H}{W}\right)\right] \quad (5)$$

Combining all of these relationships and extending the model to consider strain in both dimensions yields the final relationship:

$$P = E\left(\frac{l_W - W}{l_W} + \frac{l_L - L}{l_L}\right) \quad (6)$$

The variable l_W represents the path length of the membrane across the width of the valve, and the variable l_L represents the path length of the membrane across the length of the valve. Here, we use the post-reflow valve widths determined by profilometry as the valve width (W), and the design width of the control channel as the valve length (L).

Thick spring model. In the thick spring model, the valve membrane is modelled as a suspension bridge hanging across the channel. As always, the pressure can be expressed in terms of the force on the valve and the valve area:

$$F_1 = PWL \quad (7)$$

At equilibrium, this force is balanced out by the vertical projections of the force F_2 along the cables. Considering only one dimension yields

$$F_1 = 2F_2\sin(\theta) = 2F_2\frac{H}{\sqrt{H^2 + W^2/4}} \quad (8)$$

:

The cross-sectional area of the spring is given by hW, so we can rewrite eqn (2) here as:

$$F_2 = EhL\varepsilon \quad (9)$$

Substituting this into eqn (8) and adding in the explicit expression for F_1 from eqn (7):

$$P = \frac{2Eh}{L}\frac{H}{\sqrt{H^2 + W^2/4}}\left[\frac{l_W - W}{l_W}\right] \quad (10)$$

Finally, extending this to consider both dimensions yields a final expression of (eqn 11):

$$P = \frac{2Eh}{L}\frac{H}{\sqrt{H^2 + W^2/4}}\left[\frac{l_W - W}{l_W}\right] + \frac{2Eh}{W}\frac{H}{\sqrt{H^2 + L^2/4}}\left[\frac{l_L - L}{l_L}\right] \quad (11)$$

As before, we use the post-reflow valve widths determined by profilometry as the valve width (W), and the design width of the control channel as the valve length (L).

For each model, we generated an initial value for the Young's modulus by fitting the data with the appropriate equation while treating this value as a free parameter. We then performed a linear regression between predicted and measured values and adjusted the value for the Young's modulus by the linear regression slope to maximize agreement between predicted and measured values.

Results and discussion

Designing a microfluidic device for comprehensive characterization of tall valve geometries

The desired length and width of a rounded valve feature can be completely defined by a limited number of parameters. In general, the width of the rounded valve (F_w) should exactly match the width of the flow channel on either side to ensure a seamless joint. The length of the rounded valve depends on several parameters, including the width of the crossing control channel (C_w), the desired overlap between the two flow channel photoresists (O, overlap between AZ50 XT and SU-8), and the spacing between the crossing control channel and the beginning of the rounded valve (S) (Fig. 1C). Having a sufficiently long photoresist overlap is very important to avoid discontinuities in the height of the channel across the joint, as the AZ50 XT also rounds along the axis of the channel.

To comprehensively characterize valves encompassing a wide range of practically useful dimensions, we designed and fabricated a device with rounded valves of various common flow channel widths (50 μm, 75 μm, 100 μm, 150 μm, 200 μm, and 250 μm) crossed by control channels either 1 x or 1.5 x the valve width (Fig. 1E, Fig. 1F). For each flow and control channel width combination, we then calculated valve lengths assuming a desired spacing of either 25 μm, 50 μm, or 100 μm between the crossover control channel and the rounded photoresist feature, and desired overlaps of either 25 μm, 50 μm, 100 μm, 200 μm, or 300 μm between the two flow channel photoresists (Table S1†). To facilitate ease of fabrication and device labeling, we then chose a representative series of valve lengths encompassing both the minimum and maximum calculated lengths, with multiple values in between (Table S2†).

Valve height after reflow depends strongly on feature geometry

In prior experiments, we had begun to suspect that final valve channel heights after photoresist reflow depended not only on the photoresist spin speed, but also on the valve geometry. To characterize this phenomenon in detail, we used a profilometer to measure flow layer valve channel heights both before and after photoresist reflow for PDMS molding masters with channel sections made of AZ50 XT photoresist spun at 500 rpm, 750 rpm, 1000 rpm, 1250 rpm, and 1500 rpm. As expected, the mean feature height before hard baking depended mainly on spin speed, with lower spin speeds producing taller features (Fig. 2A). Although the mean feature height remained unchanged after hard baking (Fig. 2A, Fig. 2B), the variance of these measurements increased significantly (from ~3% of the mean to ~15% of the mean).

To understand the cause of this increased variance, we examined the dependence of feature height on the designed feature width (Fig. 2C). Before hard baking and reflow, feature heights showed no dependence on design width and depended only on the photoresist spin speed (Fig. 2C, left). After hard baking and reflow, feature heights showed a strong dependence on feature width (Fig. 2C, right). For all spin speeds, narrow features appeared to become shorter after reflow, while wider features appeared to become slightly taller (Fig. 2D). This effect plateaued at larger valve widths, with the inflection point determined by the cross-sectional aspect ratio of the valves (Fig. 2C, 2D).

Next, for each photoresist spin speed and feature width, we examined whether the final post-bake feature height showed any

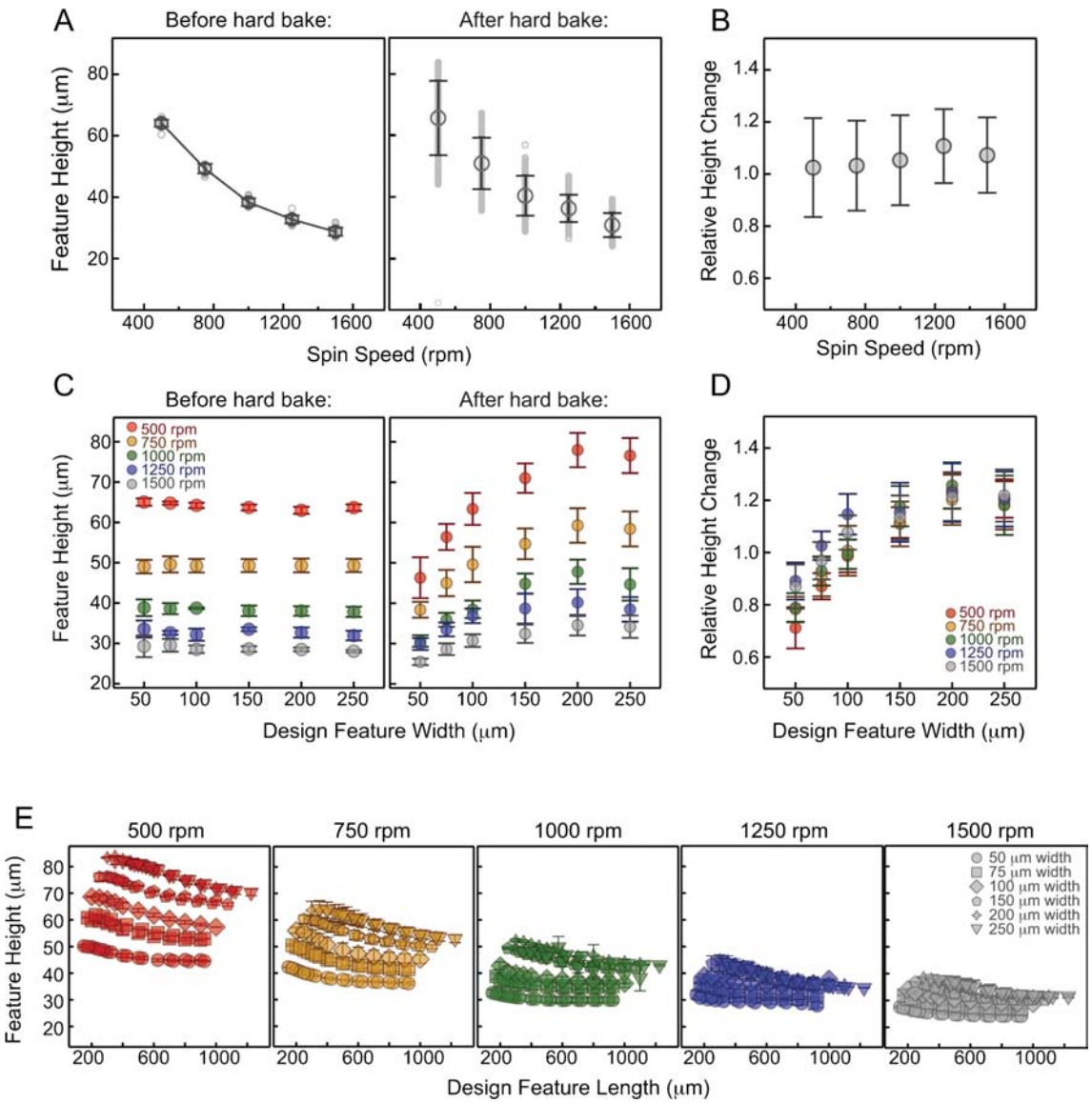

Fig. 2 Effects of heat-induced reflow on rounded feature heights. (**A**) Feature heights as a function of spin speeds for features before (left) and after (right) reflow. Light grey circles show individual valve height measurements, dark grey circles show average feature heights for each spin speed. (**B**) Change in average feature height after reflow as a function of spin speed. Change is expressed as the ratio of average heights. (**C**) Average feature heights as a function of design feature width for each spin speed before (left) and after reflow (right). (**D**) Change in average feature height after reflow as a function of both design feature width and spin speed. (**E**) Feature heights as a function of both design feature widths and lengths for each spin speed after reflow. All error bars correspond to the standard deviation of the measurements.

dependence on feature length (Fig. 2E). For all features at all spin speeds, shorter features tended to be a bit taller; this effect was more pronounced for lower spin speeds and narrower features (Fig. 2E).

Photoresist rounding after reflow also affects lateral feature dimensions

Having smooth junctions between rounded AZ50 XT features and square SU-8 features within valve channels requires matching both channel heights and widths between the two photoresist layers. To facilitate matching widths, we compared valve widths measured both before and after reflow using automated image analysis of valve photographs (Fig. 3A) and profilometry (Fig. 3B). Profilometry measurements prior to hard baking displayed a trapezoidal profile due to the conical shape of the profilometer stylus (the edges of the stylus tip touch the top corners of the photoresist, making it impossible to measure the real angle of the channel walls); consequently, we report here the pre-bake width of the profile base (“maximum width”) and the width of the profile top (“minimum width”), as well as the width as determined by image analysis (“image width”). Both before and after hard baking, maximum widths and image widths are significantly larger than the designed feature width for features up to about 200 μm, with more pronounced differences for taller features (Fig. 3C). After hard baking, the sharp corners of the photoresist disappear and no longer interfere with the taper of the profilometer stylus. As a result, the image and profilometry measurements converge, with feature base widths appearing to shrink slightly (Fig. 3D).

Nearly all of the designed device valve lengths were greater than 200 μm. Consequently, we expected measured valve lengths to be similar to design dimensions. Consistent with this, we find that measured lengths largely reflect design parameters, although the shortest valves (<300 μm) are about 10% longer than expected after reflow (Fig. S1†).

Predicting post-bake feature heights from pre-bake dimensions

A simple model relating final post-bake feature heights to pre-bake heights and feature dimensions would be a very useful tool for researchers seeking to produce rounded valve channels of a particular geometry. The measurements presented here establish that tall and narrow channels (with a large cross-sectional aspect ratio) decrease in height after baking, while low and wide channels (with a small cross-sectional aspect ratio) increase in height. A very simple model could therefore attempt to describe the ratio of pre- to post-bake feature heights (pre-bake height/post-bake height, here termed “height ratio”) as a function of only the pre-bake cross-sectional aspect ratio (measured height/width), as shown in Fig. 4A. However, a fit to this model leaves significant variance unexplained (r^2 = 0.745, sum of squared errors SSE = 8.12). Another geometrical parameter that would be expected to affect the final height is the pre-bake planar aspect ratio (measured length/width), but this is also insufficient as a sole basis for a model for the height change (Fig. 4B). Therefore, we attempted to represent the pre- to post-bake height ratio ($z \equiv h/H$) as a function of both the pre-bake cross-sectional aspect ratio (measured height/width; $x \equiv h/w$) and the pre-bake planar aspect ratio (measured length/width; $y \equiv l/w$) (Fig. S2†). This last representation can be well fitted by the following polynomial (r^2 = 0.995, SSE = 0.1605):

$$z = 0.630 + 0.175x + 0.052y + 0.742x^2 - 0.048xy \quad (12)$$

The last polynomial can be re-written as an easily-solvable quadratic equation with the pre-bake height (h) given as a function of the desired rounded height (H), pre-bake width (w), and pre-bake length (l):

$$\frac{DH}{w^2}h^2 + \left(\frac{EHl}{w^2} + \frac{BH}{w} - 1\right)h + H\left(A + \frac{Cl}{w}\right) = 0 \quad (13)$$

Where A = 0.630, B = 0.175, C = 0.052, D = 0.742, and E = −0.048. Solving this equation will provide a good approximation to the required pre-bake height needed to achieve a desired post-bake height, given a certain pre-bake width and length. However, it should be kept in mind that this is a purely empirical model based on the measurements made here. Consequently, it remains to be seen if this model can predict post-bake changes in height for features with drastically different dimensions. Additionally, baking changes the width and length of features in a way that cannot be predicted by this simple equation. To make the design of AZ50 XT features easier, we have developed an online tool that allows users to specify desired post-bake channel dimensions (available at http://derisilab.ucsf.edu under the “Software” tab). The tool calculates the appropriate pre-bake height determined by this model and looks up empirical measurements of valves that most closely match the desired dimensions. In addition, the accompanying data files are available for download (Table S3†).

Valve membrane is best modelled as a thick spring

Understanding the physics underlying valve membrane behavior is useful for effective device design and developing new microfluidic tools. A previous study by Kartalov *et al.* used a combination of theoretical and experimental approaches to characterize the relationship between closing pressures and valve dimensions for push-down microfluidic valves of various geometries.[14] For push-down valves, this relationship was best modelled by a fourth-power-polynomial superposition of three linear models: a “thick beam” model representing valve membranes as a pair of connected rigid beams in each dimension; a “thin spring” model representing membranes as semi-liquid slabs under stress; and a “thick spring” model representing membranes as suspension bridges extending across the flow channel.

Here, we examined the ability of these models to accurately predict closing pressures for significantly taller push-up microfluidic valves. To determine valve closing pressures, we connected the control channels to a pressure source, incrementally increased the pressure by either 1.72 kPa (0.25 psi) steps (for pressures below 89.6 kPa = 13 psi) or 6.9 kPa (1 psi) steps (for all other pressures), and recorded the pressure at which each valve closed. Valves were considered closed when a central portion of the valve membrane completely sealed off the flow channel (Fig. 5A). As expected, closing pressures were found to depend strongly on both flow and control channel widths, and flow

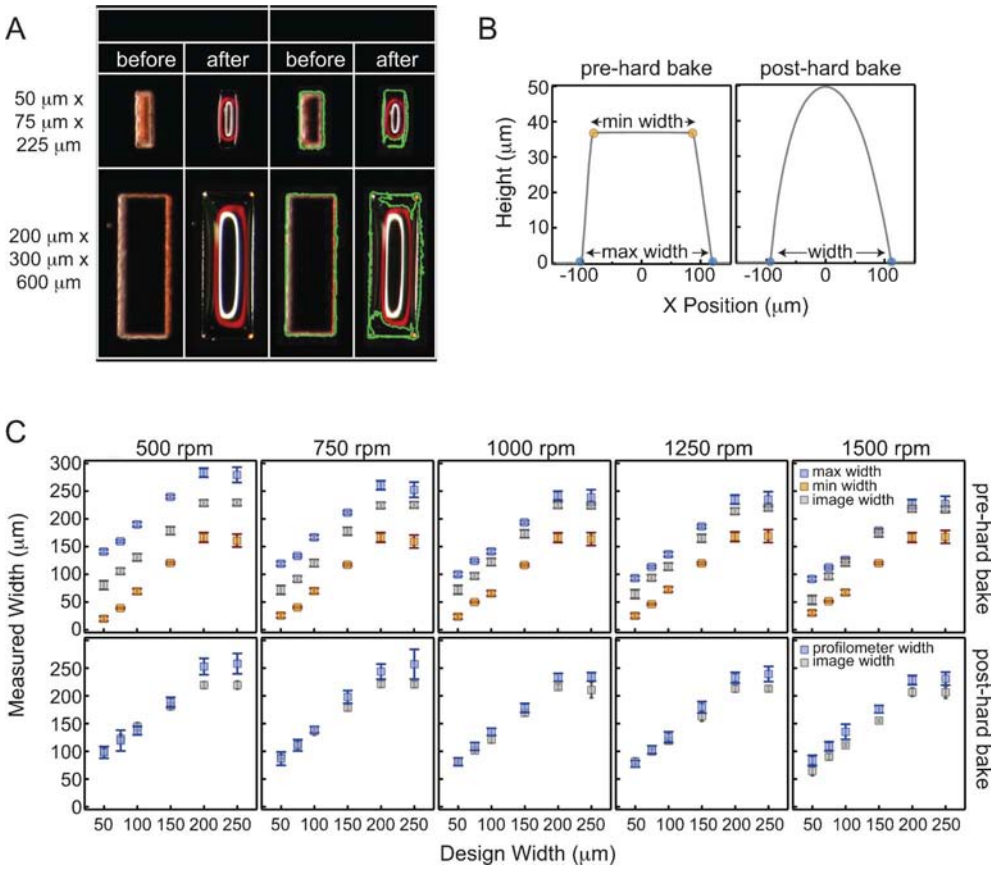

Fig. 3 Rounded feature widths before and after reflow. (**A**) Stereoscope images of two representative features before and after reflow. Right hand columns show feature edges (green) as defined by a custom edge-finding algorithm. (**B**) Profilometer data showing feature height as a function of cross-sectional position for a single valve both before (left) and after (right) reflow. Before hard baking, valve profiles are trapezoidal with both a minimum (orange) and maximum (blue) width. After baking, valve profiles are parabolic, with a single width defining the extents of the feature base (blue). (**C**) Widths measured using both image analysis and profilometry as a function of design width both before (top row) and after (bottom row) hard baking and reflow.

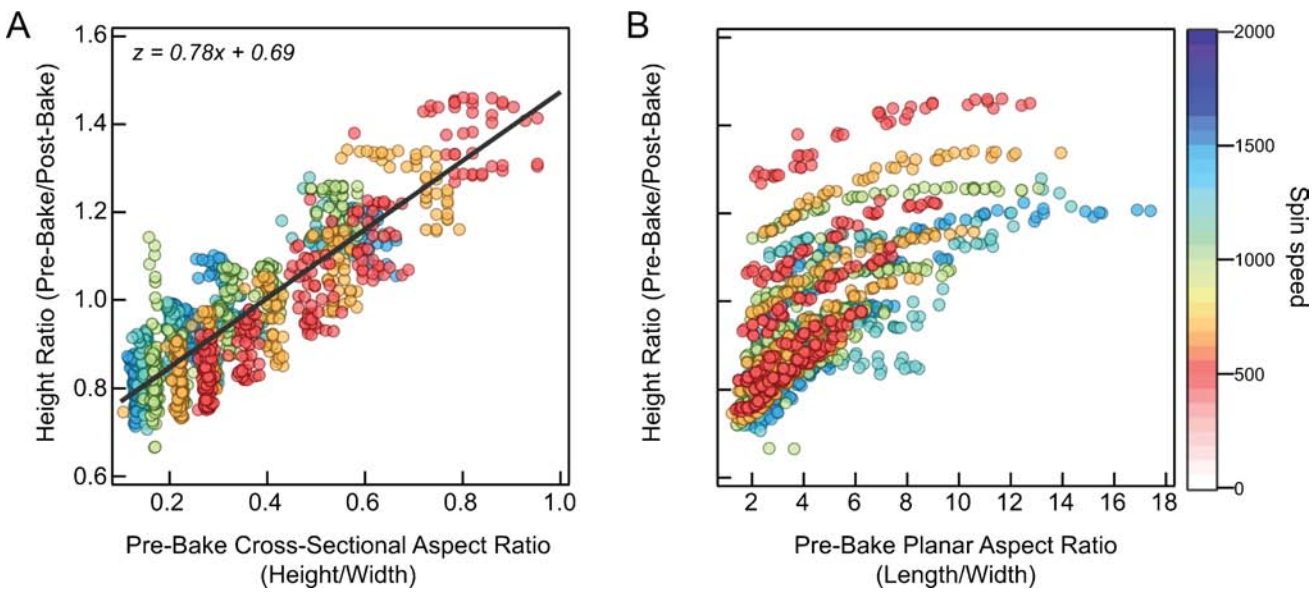

Fig. 4 Model of post-bake feature heights as a function of pre-bake aspect ratios. (**A**) Height ratio (pre-bake height/post-bake height) as a function of the pre-bake cross-sectional aspect ratio (measured height/width). The black line corresponds to the fit to the data shown on the figure. (**B**) Height ratio (pre-bake height/post-bake height) as a function of the pre-bake planar aspect ratio (measured length/width). The color of each point reflects the spin speed of the wafer.

channel height, with taller features requiring higher pressures to close (Fig. 5B). We observed two experimental failure modes. For very tall and narrow valves, valves remained open at pressures up to 413 kPa (60 psi), and higher pressures led to device delamination before valve closure could be observed. Conversely, for very short and wide valves, the valve membrane would sag and become stuck to the opposite side of the channel, rendering valves permanently open.

Two of the three models require measurement of the valve membrane thickness as an input; in addition, all three models require measured valve dimensions and the Young's modulus for PDMS. To determine membrane thickness, we imaged cross-sectional slices of 10 valves from 4 devices, yielding an average value of 15.3 $\pm$ 2.5 μm (mean $\pm$ standard deviation) (Fig. 5B). The Young's modulus of PDMS is dependent on the ratio of the two PDMS components, and ranges from 359.9 kPa (52.2 psi) for a 1 : 20 (cross-linker : elastomer base) mixture to 868.8 kPa (125.9 psi) for a 1 : 5 mixture.[16] In our fabrication process, the thick flow layer (1 : 5) and the thin control layer (1 : 20) are partially cured and then bonded by putting them in contact with each other and baking at 80 °C for at least 1 h. During this bake, excess curing agent from the flow layer diffuses into the control layer and cross-links the interface to form a single slab of PDMS (thereby changing the composition of the thin control layer). Since the Young's modulus for the PDMS membrane forming the valves is unknown, we treat this value as a free parameter in this analysis.

To evaluate each model, we calculated predicted closing pressures for each valve on the device using eqn (1), (6), and (11) and then compared these predicted values with measured closing pressures. Models were evaluated using two criteria: (1) whether predicted and measured pressures appeared to be linearly related, and (2) whether the returned value for the Young's modulus agreed with known experimental values.[16] The thick spring model tended to both underestimate the closing pressures at low pressures and overestimate closing pressures at high pressures. In addition, this model returned a vastly inflated value for the Young's modulus (39 MPa = 5598 psi). The thin spring model performed slightly better, returning a low but more reasonable value for the Young's modulus (214 kPa = 31 psi). However, the model overestimated closing pressures at low pressures and underestimated closing pressures at higher

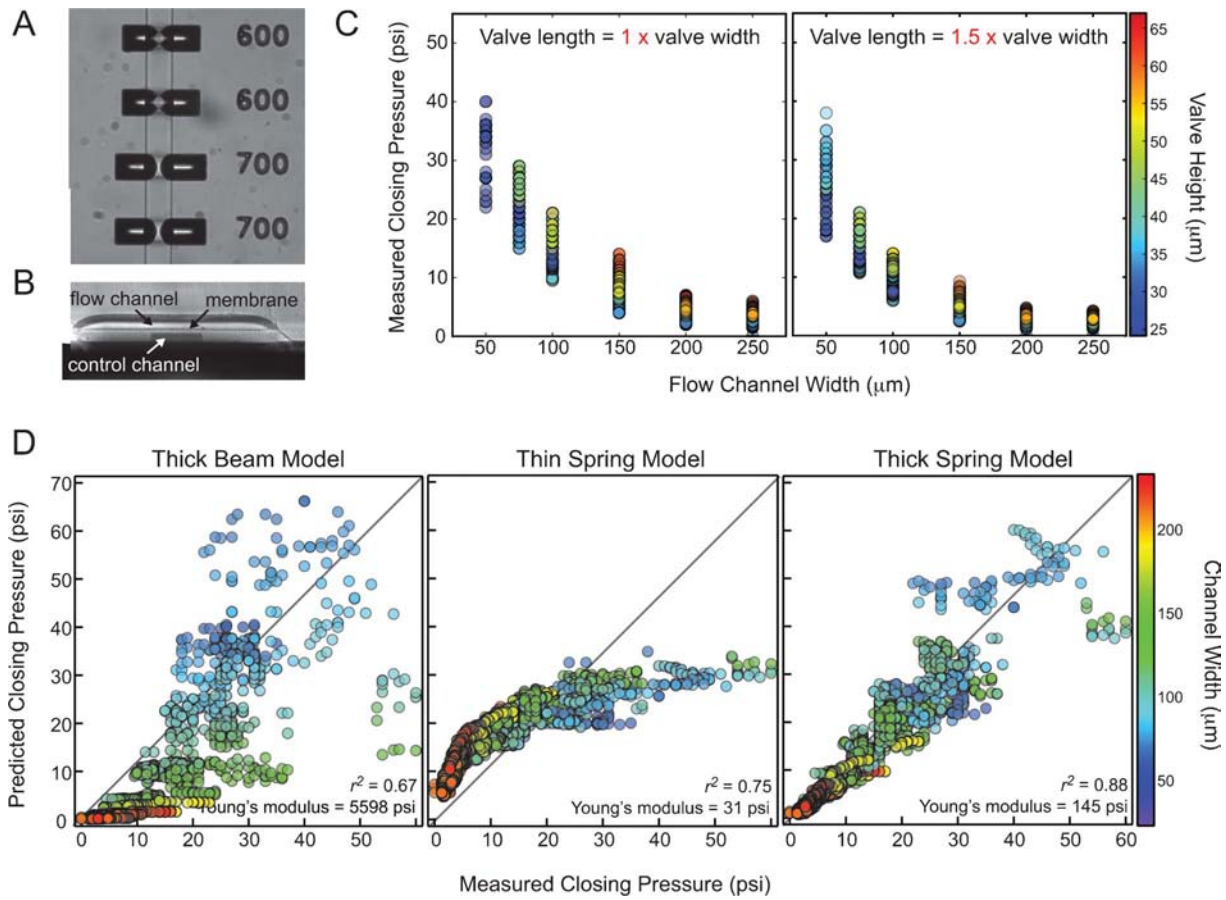

Fig. 5 Microfluidic "push-up" valves are best modelled as suspension bridges using a "thick spring" model. (**A**) Photograph showing six valves of different lengths with a single pressure applied across all of them. The 700 μm long valves are closed completely, but the 600 μm valves are not. (**B**) Microscope image of a single push-up valve in cross-section showing the flow channel, control channel, and membrane separating them. (**C**) Measured closing pressure as a function of flow channel width for control valves that are either the same width as the flow channel (left panel), or 1.5 times as wide as the flow channel (right panel). The color of each data point corresponds to the measured flow channel/valve height. (**D**) Predicted closing pressures plotted *versus* actual measured closing pressures for 3 different physical valve models: thick beam model (left), thin spring model (middle), and thick spring model (right). The color of each data point corresponds to the measured flow channel width.

pressures. Surprisingly, a version of the thick spring model optimized here for taller valve heights completely recapitulated all measured pressures and returned a value for the Young's modulus (1 MPa = 145 psi) that is very close to the experimentally measured value for a 1 : 5 mixing ratio of PDMS. Given that we expect the excess cross-linker within the 4 mm thick layer of 1 : 5 PDMS in the flow layer to diffuse into the very thin (~30 μm) 1 : 20 PDMS in the control layer, making this thin layer effectively a 1 : 5 mixture, this value is in remarkable agreement with theoretical predictions. These results suggest that push-up valves behave fundamentally differently than push-down valves, and can be explained by a simple thick spring model with no need for linear superposition.[14] Importantly, this simple relationship only becomes apparent after taking into account the profound effects of the reflow process on all of the valve dimensions.

Conclusions

Proper design and fabrication of microfluidic devices with on-chip valves requires careful consideration of the effects of the photoresist reflow process on both valve dimensions and final closing pressures. The systematic measurements presented here show that photoresist width, length, and height can change dramatically, and in a complex way, when the photoresist is rounded by baking. We have aggregated these measurements into a practical framework and software tool for choosing appropriate design parameters to create devices with the desired final valve geometries and closing pressures. In addition, these measurements allowed us to extend a "suspension bridge" ("thick spring") physical model to the deflection of "push up" valves, from which it is possible to extract good predictions of valve closing pressures for a given valve geometry. This model is very different from that previously used to describe "push down" valves.[14]

Acknowledgements

We thank Colin Campbell for assistance photographing microfluidic devices, and Kurt Thorn for assistance with membrane thickness measurements. P.M.F. was supported by a fellowship administered jointly by the Helen Hay Whitney Foundation and the Howard Hughes Medical Institute. R.G.-S. acknowledges generous support from the Engineering Division, Lawrence Berkeley National Laboratory.

References

1 T. Thorsen, S. J. Maerkl and S. R. Quake, Microfluidic large-scale integration., *Science*, 2002, **298**, 580.
2 J. Melin and S. R. Quake, Microfluidic large-scale integration: the evolution of design rules for biological automation, *Annu. Rev. Biophys. Biomol. Struct.*, 2007, **36**, 213–231.
3 T. Kalisky, P. Blainey and S. R Quake, Genomic Analysis at the Single-Cell Level., *Annu. Rev. Genet.*, 2011, **45**, 431–445.
4 P. Dalerba, *et al.* Single-cell dissection of transcriptional heterogeneity in human colon tumors., *Nat. Biotechnol.*, 2011, **29**, 1120–1127.
5 C. L. Hansen, S. Classen, J. M. Berger and S. R. Quake, A Microfluidic Device for Kinetic Optimization of Protein Crystallization and In Situ Structure Determination., *J. Am. Chem. Soc.*, 2006, **128**, 3142–3143.
6 S. J. Maerkl and S. R. Quake, A Systems Approach to Measuring the Binding Energy Landscapes of Transcription Factors., *Science*, 2007, **315**, 233–237.
7 P. M. Fordyce, *et al.* De novo identification and biophysical characterization of transcription-factor binding sites with microfluidic affinity analysis., *Nat. Biotechnol.*, 2010, **28**, 970–975.
8 R. Gomez-Sjoberg, A. A. Leyrat, D. M. Pirone, C. S. Chen and S. R. Quake, Versatile, Fully Automated, Microfluidic Cell Culture System., *Anal. Chem.*, 2007, **79**, 8557–8563.
9 M. A. Unger, H. P. Chou, T. Thorsen, A. Scherer and S. R. Quake, Monolithic microfabricated valves and pumps by multilayer soft lithography., *Science*, 2000, **288**, 113.
10 J. Liu, B. A. Williams, R. M. Gwirtz, B. J. Wold and S. Quake, Enhanced Signals and Fast Nucleic Acid Hybridization By Microfluidic Chaotic Mixing., *Angew. Chem., Int. Ed.*, 2006, **45**, 3618–3623.
11 H. P. Chou, M. A. Unger and S. R. Quake, A microfabricated rotary pump., *Biomed. Microdevices*, 2001, **3**, 323–330.
12 Z. Hua, *et al.* A versatile microreactor platform featuring a chemical-resistant microvalve array for addressable multiplex syntheses and assays., *J. Micromech. Microeng.*, 2006, **16**, 1433–1443.
13 V. Studer, Scaling properties of a low-actuation pressure microfluidic valve., *J. Appl. Phys.*, 2004, **95**, 393.
14 E. P. Kartalov, A. Scherer, S. R. Quake, C. R. Taylor and W. F. Anderson, Experimentally validated quantitative linear model for the device physics of elastomeric microfluidic valves., *J. Appl. Phys.*, 2007, **101**, 064505.
15 J. S. Marcus, W. F. Anderson and S. R. Quake, Microfluidic Single-Cell mRNA Isolation and Analysis., *Anal. Chem.*, 2006, **78**, 3084–3089.
16 D. Armani, C. Liu and N. Aluru, Re-configurable fluid circuits by PDMS elastomer micromachining., *Technical Digest. IEEE International MEMS 99 Conference. Twelfth IEEE International Conference on Micro Electro Mechanical Systems (Cat. No.99CH36291)*, 1999, 222–227.